CHINESE OPTICS LETTERS

Vol. 21, No. 1 | January 2023

Design of an optical slot waveguide amplifier based on Er^{3+}-doped tellurite glass

Ning Wei (卫 宁)[1,2], Xiaobo Li (李晓博)[1,2], Jiajing He (何佳晶)[1,2], Yongtao Fan (范永涛)[1,2], Yaping Dan (但亚平)[3], and Jun Wang (王 俊)[1,2,4,5*]

[1] Laboratory of Micro-Nano Optoelectronic Materials and Devices, Key Laboratory of Materials for High-Power Laser, Shanghai Institute of Optics and Fine Mechanics, Chinese Academy of Sciences, Shanghai 201800, China

[2] Center of Materials Science and Optoelectronics Engineering, University of Chinese Academy of Sciences, Beijing 100049, China

[3] University of Michigan-Shanghai Jiao Tong University Joint Institute, Shanghai Jiao Tong University, Shanghai 200240, China

[4] CAS Center for Excellence in Ultra-intense Laser Science (CEULS), Shanghai 201800, China

[5] State Key Laboratory of High Field Laser Physics, Shanghai Institute of Optics and Fine Mechanics, Chinese Academy of Sciences, Shanghai 201800, China

*Corresponding author: jwang@siom.ac.cn

Received May 5, 2022 | Accepted July 22, 2022 | Posted Online September 21, 2022

The idea of a slot waveguide amplifier based on erbium-doped tellurite glass is first theoretically discussed in this work. Choosing the horizontal slot for low propagation loss, the TM mode profile compressed in the insertion layer was simulated, and the gain characteristics of the slot waveguide amplifier were calculated. Combining the capacity to confine light locally and the merits of tellurite glass as an emission host, this optimized amplifier shows enhanced interactions between the electric field and erbium ions and achieves a net gain of 15.21 dB for the 0.01 mW input light at 1530 nm, implying great promise of a high-performance device.

Keywords: guided waves; optical amplifiers; rare-earth-doped materials.

DOI: 10.3788/COL202321.011404

1. Introduction

Enabling the construction of complex optoelectronic systems in a reliable and cost-effective way, the potential of photonic integrated circuits (PICs) is now explored in many applications, such as optical communication[1,2], computing[3], sensing[4], and detecting[5]. There has been substantial progress achieved in recent years, however, transmission loss resulting from absorption, reflection, diffraction, scattering, or coupling efficiency remains a key challenge to improve the functionalities of integrated devices[6–8]. Limited by the fabrication technologies as well as material platforms, the attenuation of light energy at the interface is inevitable and not negligible, which should be compensated by optical amplification to ensure adequate power efficiency, signal noise ratio, or quality factor.

Inspired by the great success of erbium-doped fiber amplifiers (EDFAs) in optical telecommunication, erbium-doped waveguide amplifiers (EDWAs) have attracted much attention in decades[9]. Compared to semiconductor optical amplifiers (SOAs) based on electron–hole pairs recombination in III–V semiconductors, EDWAs can offer longer excited-state lifetime, simpler structure, lower noise, broader bandwidth, and thermally stabler optical gain, allowing for high-speed amplification[9,10]. Despite the fact that Er ions interactions and clustering effects constrain the dopant concentration, highly Er^{3+}-doped active materials are still sought to accomplish greater maximum gain, which makes waveguide amplifiers more competitive. Hence, significant investigations on host materials, co-dopant addition proportion, and fabrication techniques of EDWAs have been conducted. Glass hosts exhibit broad smooth emission spectra of Er^{3+} and good thermal stability, more suitable to develop a broadband amplifier than crystal or polymer. Among all glass host matrices, tellurite glass offers a number of advantages because of its high-refractive-index enabling compact devices, wide emission bandwidth, large emission cross section, low cross-relaxation coefficient, lower phonon energy, relative independence of the 1550 nm Er lifetime on concentration, and high Er solubility, as has been demonstrated in fiber amplifiers[11–15]. To combine the outstanding gain material with the mature silicon-on-insulator (SOI) platform for the realization of a practical EDWA, an Er-doped tellurite glass amplifier based on a silicon slot waveguide is proposed in our work.

Slot waveguides are of high interest in integrated optics owing to their ability to confine light strongly in a very thin low-refractive-index region. For this reason, they have shown great potential to produce high-performance integrated waveguide lasers and amplifiers[16–19]. But, a vertical slot fabrication

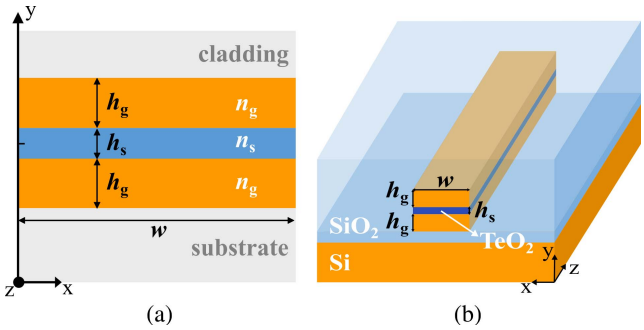

Fig. 1. Structure of slot waveguide. (a) Two-dimensional schematic of horizontal slot waveguide; (b) three-dimensional schematic of horizontal slot waveguide.

involves etching in a very narrow region, which can cause severe roughness in the waveguide sidewall in contrast to the precise and easy height control of the deposition layer in current micro/nanofabrication technologies; as a result, a horizontal slot is more favorable in the EDWA design for its lower propagation loss[20,21]. In this paper, a 40 nm thick horizontal slot of TeO_2:Er^{3+} sandwiched by two high-index silicon strips is employed. Due to the electric displacement continuity boundary condition, the electric field of quasi-TM polarized light in the optically thinner medium will be enhanced by the factor of n_g^2/n_s^2 (Fig. 1). The Er-doped tellurite glass is filled into the slot as the core layer, and a four-level spectroscopic model pumped at 1480 nm is presented. By accurate optimization for the slot and calculation of gain characteristics, we demonstrate theoretically a 4 cm long EDWA with a net gain up to 15 dB for 1480 nm pump light, whose Er^{3+} concentration is 2.2×10^{26} m^{-3}.

2. Design of the Slot Waveguide

Since active material exists in the slot region only, a waveguide in which pump and signal light is more concentrated in the low-refractive-index area is desired for higher energy availability. Also, a higher electric field intensity in the active material is needed for a stronger light–matter interaction. The trade-off of these two requirements implies that the structure of the slot waveguide used for amplification should be carefully designed, according to the mode distribution. In this work, the COMSOL software based on the finite element method (FEM) was used to simulate the modal distribution and optimize the waveguide structure. A two-dimensional model was built in the Wave Optics Module, coupled with the Electromagnetic Waves Frequency Domain (ewfd) interface, and studied by Mode Analysis solver. The schematics of the slot waveguide with horizontal sidewalls are displayed in Fig. 1. An image of the cross section of the sandwiched waveguide is shown in Fig. 1(a), and that in the 3D view is shown in Fig. 1(b). An Er-doped TeO_2 glass layer with the height h_s is inserted into the two silicon strip waveguides with the same height h_g and width w as the gain medium. Outside the sandwich-structured silicon strip, the cladding and substrate materials are both silica. The three geometric parameters h_s, h_g, and w are focused on the following optimization.

Table 1. Refractive Indices Used in Simulation[22,23].

Material	Index at 1530 nm	Index at 1480 nm
Si	3.478	3.482
SiO_2	1.444	1.451
TeO_2:Er^{3+}	2.06	2.07

Considering the overlap between the signal and pump beam, the modal profile should be simulated at both λ_s (1530 nm) and λ_p (1480 nm). The refractive indices of waveguide materials chosen for simulation are shown in Table 1. The refractive index variation of TeO_2:Er^{3+} owing to dopant concentration is neglected for its relatively small influence[22,24]. The modal profiles of electric field $E(x, y)$ in the slot waveguide simulated at 1530 and 1480 nm are depicted in Fig. 2. From the simulation results, we can see that the horizontal slot waveguide is strongly polarization-sensitive: the enhanced electric field component of the y direction (E_y), which is perpendicular to the interface, causes the domination of the TM mode in the slot region. Thus, only the TM mode contributes to the amplification process.

To coordinate the two requirements in a more quantitative way, we define two figures of merit as follows: the light field confinement factor (Γ_s) in the slot region

$$\Gamma_s = \frac{\iint_{slot} |E(x,y)|^2 dxdy}{\iint_{total} |E(x,y)|^2 dxdy}, \tag{1}$$

and the normalized power density (I_{norm})[25,26]

$$I_{norm} = \frac{\Gamma_s}{h_s w}. \tag{2}$$

Γ_s represents the percentage of light energy transmitting in the slot, the part really utilized during the amplification process. Although a larger Γ_s is preferred, the high-energy proportion in the gain medium does not actually mean a strong light intensity, which directly determines rate of stimulated absorption or emission. To obtain the highest gain amplification, therefore, we should optimize the structure of the slot waveguide, taking both Γ_s and I_{norm} into account.

As a prominent factor of slot waveguide functionality, the value of slot height h_s is chosen first, then sweeping parameters of h_g and w simultaneously to find the optimal variables relevant to specific h_s. Before optimization, we assumed the $h_g = 200$ nm and $w = 300$ nm, two moderate values acquired from previous articles[27,28]. The dependences of the effective refractive index (n_{eff}), Γ_s, and I_{norm} on h_s are simulated at 1530 nm and 1480 nm under the presumption, as shown in Fig. 3. Because a high n_{eff}

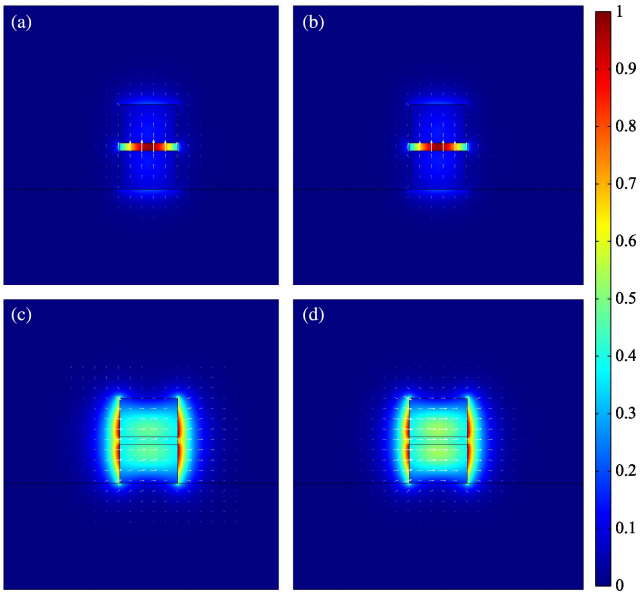

Fig. 2. Distribution of normalized $|E(x, y)|$ in slot waveguide with the Si guiding layer height h_g = 200 nm, width w = 300 nm, and slot height h_s = 40 nm. (a) TM mode profile at 1530 nm; (b) TM mode profile at 1480 nm; (c) TE mode profile at 1530 nm; (d) TE mode profile at 1480 nm. The white arrows represent the directions and amplitudes of the electric field in the *xy* plane.

usually means a high-energy proportion of the corresponding mode, the relationship $n_{\text{eff}}(\text{TM}) > n_{\text{eff}}(\text{TE})$ is always requested throughout the design process. Apparently, from Fig. 3(a), the slot guiding structure supports a higher confinement in the slot region for the TM mode than that for the TE mode. Both the pump and signal light are confined in the slot under TM mode, and their interaction with the Er ion is enhanced in the slot, which will be beneficial for achieving higher gain. But, it is noted that Γ_s and I_{norm} show distinct changes with the increasing h_s in Figs. 3(b) and 3(c). As the height of the low-refractive-index region rises, more light energy flows into the slot; but, the average power density reduces in the increasing area. For maximizing the light–matter interaction and minimizing the energy waste, therefore, a modest value $h_s = 40\,\text{nm}$ is set in our EDWA design to reach a compromise; since a proper value ranges from 20 to 60 nm, where the curves in Figs. 3(b) and 3(c) change from the maximum to half.

The silicon layer height h_g and width w also need a trade-off between the two figures of merit. The relationships of Γ_s with the two parameters are illustrated in Fig. 4(a). It is revealed that Γ_s increases monotonically with w, but there is a maximum along with a heightening h_g. The explanation of this phenomenon is that a wide w can alleviate the mode leakage in the $Si(TeO_2)$-SiO_2 interface, allowing more optical power to be accommodated in the waveguide; naturally, for the constant ratio of slot area to the waveguide's, Γ_s will keep increasing when widening w. However, an excessive w in practice will lead to a proportional loss in the slot waveguide. Besides, the TE mode will gradually turn dominant like the eigenmode in a planar waveguide as the waveguide becomes flatter, which causes the w to be correctly selected. A similar alleviation of light leaking happens as well when increasing h_g moderately, since the two strips with low height cannot confine the light in the slot and silicon layer well. But, continuing to increase the h_g causes the reduction of the ratio of slot area to the whole cross section, and higher portions of light spread over the silicon strip. So, Γ_s tends to saturate and even decrease. In Fig. 4(b), I_{norm} is inversely related to w, while the change from h_g resembles Γ_s's. According to above results, w is appropriately determined to be 300 nm, and the corresponding optimal h_g is 200 nm, showing that our prior assumption is reasonable.

3. Gain Characteristics of Slot Waveguide Amplifier

Supported by the optimization of the waveguide, the Er-doped low-refractive-index material is filled into the slot waveguide, and the potential gain of the slot waveguide amplifier is investigated. The gain characteristic analysis is based on the Er^{3+}-doped four-level model, as shown in Fig. 5, and pumping at 1480 nm was chosen owing to the excessive absorption in the silicon layers and high excited-state absorption (ESA) of Er at 980 nm[29]. To achieve a more accurate simulation, the cooperative up-conversion (C_{up}), cross relaxation (C_{14}), and

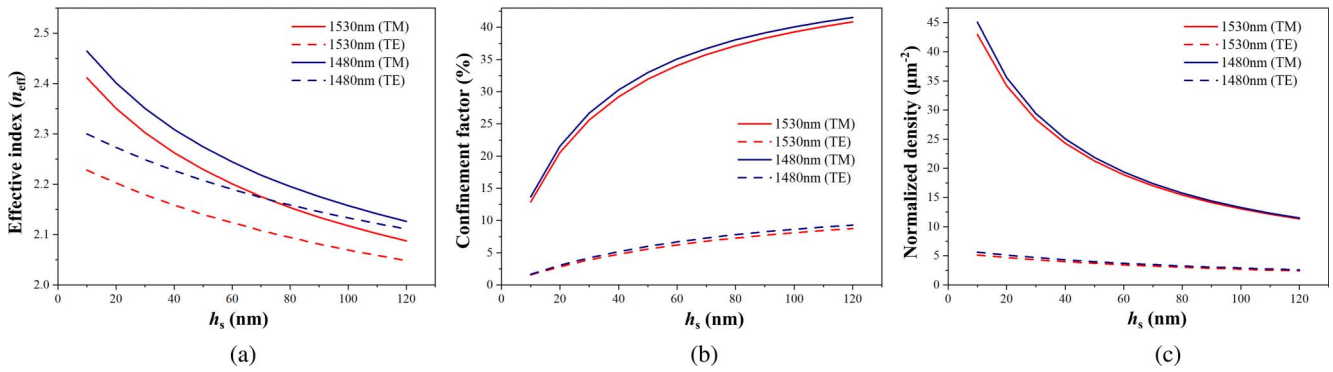

Fig. 3. Simulation results for varying h_s from 10 to 120 nm. (a) Effective refractive indices n_{eff} of the TM/TE mode at 1530 nm and 1480 nm; (b) confinement factors Γ_s of the TM/TE mode at 1530 nm and 1480 nm; (c) normalized power density I_{norm} of the TM/TE mode at 1530 nm and 1480 nm.

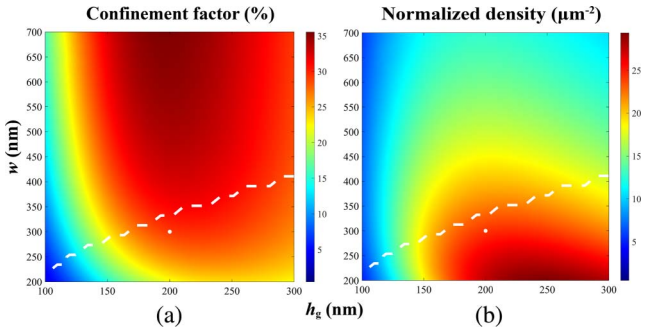

Fig. 4. Optimization of width and height of the Si layer with a 40 nm thick slot. (a) Field confinement factors Γ_s as a function of single silicon layer height h_g and waveguide width w. (b) Normalized power density I_{norm} as a function of single silicon layer height h_g and waveguide width w. The white dashed lines in (a) and (b) are the boundaries of the n_{eff} (TM) > n_{eff} (TE) condition; only the domains below these lines are valid. The white dots in (a) and (b) denote Γ_s = 29.17% and I_{norm} = 24.31 μm^{-2}, respectively, at the positions of h_g = 200 nm and w = 300 nm.

spontaneous emission (A_{43}, A_{32}, A_{21}) are involved. The operational principle of the amplifier pumped at 1480 nm is as follows: the Er^{3+} ions in the ground state absorb the photons and then are excited from the ground $^4I_{15/2}$ level to the higher Stark split sub-levels in $^4I_{13/2}$. Due to thermal relaxation, the excited ions rapidly decay to the lower, metastable sub-levels of $^4I_{13/2}$. When the pump power exceeds the threshold power, population inversion is built between $^4I_{15/2}$ and $^4I_{13/2}$. Then, the rate of stimulated emission at 1530 nm caused by signal light overtakes the opposite stimulated absorption process, so the device realizes the light amplification. Here, the amplified spontaneous emission (ASE) was neglected. Combined with the ion interactions induced energy-level transitions, the simplified versions of the rate equations can be expressed by

$$\frac{dN_1}{dt} = -(W_{12} + R_{12})N_1 + (W_{21} + R_{21} + A_{21})N_2 + C_{up}N_2^2 - C_{14}N_1N_4, \quad (3)$$

$$\frac{dN_2}{dt} = (W_{12} + R_{12})N_1 - (W_{21} + R_{21} + A_{21} + R_{24})N_2 + A_{32}N_3 - 2(C_{up}N_2^2 - C_{14}N_1N_4), \quad (4)$$

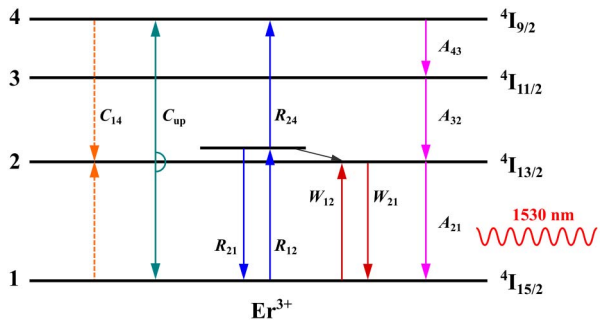

Fig. 5. Energy-level transitions for the Er^{3+}-doped four-level system (pumped by 1480 nm).

$$\frac{dN_3}{dt} = -A_{32}N_3 + A_{43}N_4, \quad (5)$$

$$\frac{dN_4}{dt} = R_{24}N_2 - A_{43}N_4 + C_{up}N_2^2 - C_{14}N_1N_4, \quad (6)$$

$$N_{Er} = N_1 + N_2 + N_3 + N_4, \quad (7)$$

where N_1, N_2, N_3, and N_4 are defined as the concentrations of Er^{3+} in the $^4I_{15/2}$, $^4I_{13/2}$, $^4I_{11/2}$, and $^4I_{9/2}$ energy states, respectively. N_{Er} is the total Er^{3+} ion concentration. Supposing all Er^{3+} ions are uniformly doped and optically sensitized, the rate equations are analyzed under steady-state conditions of the population densities and solved using the method of overlap integral and an iteration method coupled with the propagation equations of the signal and the pump power, described by

$$\frac{dP_s}{dz} = \Gamma_s[\sigma_{21}(\nu_s)N_2 - \sigma_{12}(\nu_s)N_1]P_s - \alpha_s P_s, \quad (8)$$

$$\frac{dP_p}{dz} = \Gamma_p[\sigma_{21}(\nu_p)N_2 - \sigma_{24}(\nu_p)N_2 - \sigma_{12}(\nu_p)N_1]P_p - \alpha_s P_p. \quad (9)$$

The meanings and the values of the relevant parameters are shown in Table 2. Because it is difficult to test accurately all the parameters of the active material used in the simulation, the values in Table 2 are mainly accumulated from recent researches[11,29]. The 2.2×10^{26} m^{-3} dopant concentration and the 1 dB/cm loss coefficients of horizontal slot waveguide are typical amounts related to the promising reactive co-sputtering

Table 2. Parameter Values of TeO_2:Er^{3+} Rate Equation Model[11,23].

Parameter	Full name	Value
N_{Er}	Erbium ion density	2.2×10^{26} m^{-3}
$\sigma_{12}(\nu_p)$	Absorption cross section at 1480 nm	3.0×10^{-24} m^2
$\sigma_{21}(\nu_p)$	Emission cross section at 1480 nm	0.4×10^{-24} m^2
$\sigma_{24}(\nu_p)$	Excited-state absorption cross section	0.85×10^{-25} m^2
$\sigma_{12}(\nu_s)$	Absorption cross section at 1530 nm	3.5×10^{-24} m^2
$\sigma_{21}(\nu_s)$	Emission cross section at 1530 nm	4.4×10^{-24} m^2
A_{21}	Spontaneous emission rate of N_2	2×10^3 s^{-1}
A_{32}	Spontaneous emission rate of N_3	2.5×10^4 s^{-1}
A_{43}	Spontaneous emission rate of N_4	10^7 s^{-1}
C_{up}	Up-conversion coefficient	2.7×10^{-24} m$^3 \cdot$ s^{-1}
C_{14}	Cross-relaxation coefficient	1.0×10^{-23} m$^3 \cdot$ s^{-1}
L_p	Propagation loss of the pump laser	1 dB/cm
L_s	Propagation loss of the signal laser	1 dB/cm

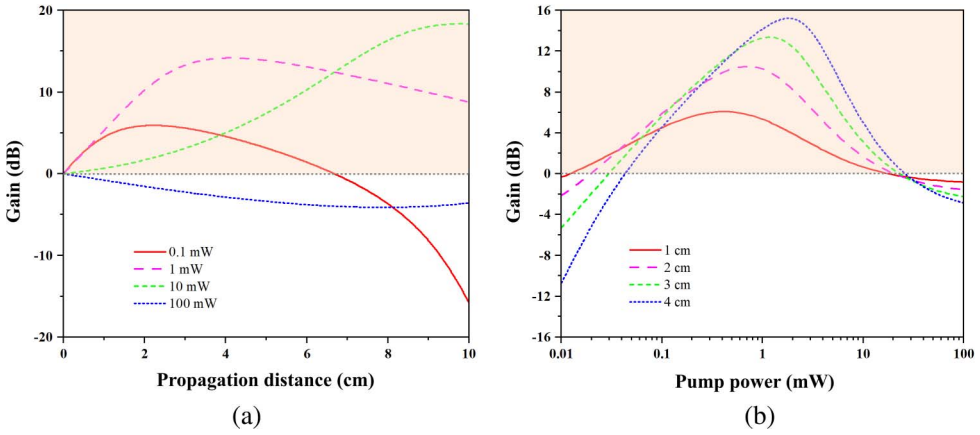

Fig. 6. Simulated gain characteristics of the designed slot waveguide amplifier. (a) Gain versus propagation distance for different pump powers. (b) Gain versus pump power for different amplifier lengths. For both situations, the signal power is assumed to be 0.01 mW.

deposition technology. The initial signal power is determined to be 0.01 mW during the whole analysis process, so the propagation equations can be worked out by MATLAB using the Runge–Kutta algorithm, thus obtaining the gain characteristics through the iterative solving strategy for two sets of equations (shown in Fig. 6).

To study the dynamics of the amplification process where the pump and signal light are input to a slot waveguide in the same direction, the change of signal power propagating in the amplifier along with pump light is shown in Fig. 6(a). As can be seen, the signal gain functions versus propagation length under 0.1, 1, and 10 mW pumping are similar: the signal power increases at first and then decreases continually, and the length shows an optimum value. The mechanism is that the gain and loss are two competitive processes in the signal light transmission, the former stemming from the stimulated emission and the latter from absorption and propagation loss in the waveguide. Therefore, population inversion is critical to steer the net effect, which depends on whether the pump power is high enough to resist various de-population processes of the $^4I_{13/2}$ level (e.g., spontaneous emission, non-radiative transition, ESA, and ion–ion interactions). Because pump power is constantly consumed in the transmission along the waveguide, after the first amplification of the small signal and reaching the optimal length, the pump power becomes smaller than the threshold power, and the amplification turns off, leaving the loss governing the subsequent propagation. Usually a high pump power is needed to achieve a longer active area and greater output gain. For instance, the optimum length and saturation output power are positively correlated to the pump power of curves pumped by 0.1, 1, and 10 mW in Fig. 6(a). But, an extremely high pump power always causes a severe ion–ion interaction, and consequently the augmented energy transfer up-conversion and ESA will degrade the gain characteristics seriously and even result in a pure "negative gain," just as in the lowest curve of Fig. 6(a). From above analysis, it is known that a too long amplifier and a too high pump power all harm the performance, so the impact of pump power on gain characteristics entails assessing for a practical application. In Fig. 6(b), the four gain functions versus pump power of different length amplifiers are nearly identical. Obviously, the optimal pump power and maximum gain increase along with the increased length, but it shows a lower threshold power for a shorter amplifier owing to the smaller accumulative propagation loss. The largest pump power our designed 2.2×10^{26} m^{-3}-doped TeO_2:Er^{3+} amplifier can endure is located at 20 mW approximately. Below the tipping point, the highest gains, which 1, 2, 3, and 4 cm long amplifiers can attain, are predicted to be 6.08, 10.49, 13.37, and 15.21 dB, respectively.

4. Conclusions

Waveguide amplifiers have always been significant components for integrated photonics. Unfortunately, the low concentration of rare earth ions doped in the host and the inadequate optimization of the waveguide structure have been the common bottleneck. In our work, the performance of the horizontal slot waveguide amplifier based on Er^{3+}-doped tellurite glass is simulated and evaluated. The modal characteristics under TE and TM modes were described. The slot structure can support a higher TM mode confined in the slot region compared to the TE mode. Despite doping the Er ions in silicon waveguide material, filling the gain medium into the horizontal slot eases the fabrication process, which is promised to be produced by reactive co-sputtering deposition. When the slot waveguide had an optimal width of 300 nm, a silicon height of 200 nm, and a slot width of 40 nm, the light field confinement factor and normalized power density in the slot region for TM polarization were 0.2917 and 24.31 μm^{-2} at 1530 nm, respectively. A four-level spectroscopic model pumped at 1480 nm was presented. The rate equations and propagation equations were solved, and the gain characteristics of the slot waveguide amplifier were numerically simulated. The primary parameters were optimized. A net gain of 15.21 dB was achieved for the signal

power of 0.01 mW at 1530 nm, pump power of 2 mW, Er^{3+} concentration of 2.2×10^{26} m^{-3}, and waveguide length of 4 cm.

Acknowledgement

This work was supported by the National Natural Science Foundation of China (NSFC) (No. 61975221) and the Shanghai Science and Technology International Cooperation Fund (No. 19520743900).

References

1. K. Liu, H. Fan, Y. Huang, X. Duan, Q. Wang, X. Ren, Q. Wei, and S. Cai, "A pair of integrated optoelectronic transceiving chips for optical interconnects," Chin. Opt. Lett. **16**, 091301 (2018).
2. E. Agrell, M. Karlsson, A. R. Chraplyvy, D. J. Richardson, P. M. Krummrich, P. Winzer, K. Roberts, J. K. Fischer, S. J. Savory, B. J. Eggleton, M. Secondini, F. R. Kschischang, A. Lord, J. Prat, I. Tomkos, J. E. Bowers, S. Srinivasan, M. Brandt-Pearce, and N. Gisin, "Roadmap of optical communications," J. Opt. **18**, 063002 (2016).
3. W. Bogaerts, D. Pérez, J. Capmany, D. A. B. Miller, J. Poon, D. Englund, F. Morichetti, and A. Melloni, "Programmable photonic circuits," Nature **586**, 207 (2020).
4. A. Hänsel and M. J. R. Heck, "Opportunities for photonic integrated circuits in optical gas sensors," J. Phys. Photonics **2**, 12002 (2020).
5. J. Fridlander, F. Sang, V. Rosborough, F. Gambini, S. T. Šuran-Brunelli, J. R. Chen, K. Numata, M. Stephen, L. A. Coldren, and J. Klamkin, "Dual laser indium phosphide photonic integrated circuit for integrated path differential absorption lidar," IEEE J. Sel. Top. Quantum Electron. **28**, 6100208 (2022).
6. A. Rahim, A. Hermans, B. Wohlfeil, D. Petousi, B. Kuyken, D. V. Thourhout, and R. Baets, "Taking silicon photonics modulators to a higher performance level: state-of-the-art and a review of new technologies," Adv. Photonics **3**, 024003 (2021).
7. L. Lu, S. Zhao, L. Zhou, D. Li, Z. Li, M. Wang, X. Li, and J. Chen, "Nonblocking silicon optical switch based on electro-optic Mach-Zehnder interferometers," Opt. Express **24**, 9295 (2016).
8. L. He, Ş. K. Özdemir, and L. Yang, "Whispering gallery microcavity lasers," Laser Photon. Rev. **7**, 60 (2012).
9. J. D. B. Bradley and M. Pollnau, "Erbium-doped integrated waveguide amplifiers and lasers," Laser Photon. Rev. **5**, 368 (2010).
10. D. R. Zimmerman and L. H. Spiekman, "Amplifiers for the masses: EDFA, EDWA, and SOA amplets for metro and access applications," J. Light. Technol. **22**, 63 (2004).
11. H. C. Frankis, H. M. Mbonde, D. B. Bonneville, C. Zhang, R. Mateman, A. Leinse, and J. D. B. Bradley, "Erbium-doped TeO_2-coated Si_3N_4 waveguide amplifiers with 5 dB net gain," Photon. Res. **8**, 127 (2020).
12. J. S. Wang, E. M. Vogel, and E. Snitzer, "Tellurite glass: a new candidate for fiber devices," Opt. Mater. **3**, 187 (1994).
13. A. Mori, Y. Ohishi, and S. Sudo, "Erbium-doped tellurite glass fibre laser and amplifier," Electron. Lett. **33**, 863 (1997).
14. Y. Ohishi, A. Mori, M. Yamada, H. Ono, Y. Nishida, and K. Oikawa, "Gain characteristics of tellurite-based erbium-doped fiber amplifiers for 1.5-μm broadband amplification," Opt. Lett. **23**, 274 (1998).
15. S. Shen, A. Jha, X. Liu, M. Naftaly, K. Bindra, H. J. Bookey, and A. K. Kar, "Tellurite glasses for broadband amplifiers and integrated optics," J. Am. Ceram. Soc. **85**, 1391 (2002).
16. V. R. Almeida, Q. Xu, C. A. Barrios, and M. Lipson, "Guiding and confining light in void nanostructure," Opt. Lett. **29**, 1209 (2004).
17. J. T. Robinson, C. Manolatou, L. Chen, and M. Lipson, "Ultrasmall mode volumes in dielectric optical microcavities," Phys. Rev. Lett. **95**, 143901 (2005).
18. C. A. Barrios and M. Lipson, "Electrically driven silicon resonant light emitting device based on slot-waveguide," Opt. Lett. **13**, 10092 (2005).
19. M. Galli, D. Gerace, A. Politi, M. Liscidini, M. Patrini, L. C. Andreani, A. Canino, M. Miritello, R. L. Savio, A. Irrera, and F. Priolo, "Direct evidence of light confinement and emission enhancement in active silicon-on-insulator slot waveguides," Appl. Phys. Lett. **89**, 241114 (2006).
20. R. Sun, P. Dong, N. Feng, C. Hong, J. Michel, M. Lipson, and L. Kimerling, "λ = 1550 nm horizontal single and multiple slot waveguides: optical transmission at λ = 1550 nm," Opt. Express **15**, 17967 (2007).
21. A. Tengattini, D. Gandolfi, N. Prtljaga, A. Anopchenko, J. M. Ramirez, F. F. Lupi, Y. Berencen, D. Navarro-Urrios, P. Rivallin, K. Surana, B. Garrido, J.-M. Fedeli, and L. Pavesi, "Toward a 1.54 μm electrically driven erbium-doped silicon slot waveguide and optical amplifier," J. Light. Technol. **31**, 391 (2013).
22. V. A. G. Rivera and D. Manzani, *Technological Advances in Tellurite Glasses: Properties, Processing, and Applications* (Springer International, 2017).
23. M. Zhang, G. Hu, S. Zhang, D. Gao, Y. Sun, and F. Wang, "Gain characteristics of the hybrid slot waveguide amplifiers integrated with NPs-PMMA covalently linked nanocomposites," RSC Adv. **10**, 11148 (2020).
24. R. A. H. El-Mallawany, *Tellurite Glasses Handbook: Physical Properties and Data*, 2nd ed. (CRC Press, 2016).
25. T. D. Visser, H. Blok, B. Demeulenaere, and D. Lenstra, "Confinement factors and gain in optical amplifiers," IEEE J. Quantum Electron. **33**, 1763 (1997).
26. N. Feng, J. Michel, and L. C. Kimerling, "Optical field concentration in low-index waveguides," IEEE J. Quantum Electron. **42**, 883 (2006).
27. P. Mullner and R. Hainberger, "Structural optimization of silicon-on-insulator slot waveguides," IEEE Photon. Technol. Lett. **18**, 2557 (2006).
28. P. Sanchis, J. Blasco, A. Martinez, and J. Marti, "Design of silicon-based slot waveguide configurations for optimum nonlinear performance," J. Light. Technol. **25**, 1298 (2007).
29. Y. Hu, S. Jiang, G. Sorbello, T. Luo, Y. Ding, B. Hwang, J. Kim, H. Seo, and N. Peyghambarian, "Cooperative upconversion in a new high-Er-doped tellurite glass," Proc. SPIE **4282**, 57 (2001).